Air-Sea Turbulent Heat Flux Feedback over Mesoscale Eddies

Sophia M Moreton[1], David Ferreira[1], Malcolm J Roberts[2], and Helene Theresa Hewitt[2]

[1]University of Reading
[2]Met Office

November 22, 2022

Abstract

Air-sea turbulent heat fluxes play a fundamental role in generating and dampening sea surface temperature (SST) anomalies. To date, the turbulent heat flux feedback (THFF) is well quantified at basin-wide scales (~20 W~m^{-2}~K^{-1}) but remains unknown at the oceanic mesoscale (10-100 km). Here, using an eddy-tracking algorithm in three configurations of the coupled climate model HadGEM3-GC3.1, the THFF over mesoscale eddies is estimated. The THFF magnitude is strongly dependent on the ocean-to-atmosphere regridding of SST, a common practice in coupled models for calculating air-sea heat flux. Our best estimate shows that the mesoscale THFF ranges between 35 and 45 W~m^{-2}~K^{-1} globally, across different eddy amplitudes. Increasing the ratio of atmosphere-to-ocean grid resolution can lead to an underestimation of the THFF, by as much as 75% for a 6:1 resolution ratio. Our results suggest that a large atmosphere-to-ocean grid ratio can result in an artificially weak dampening of mesoscale SST anomalies.

Air-Sea Turbulent Heat Flux Feedback over Mesoscale Eddies

Sophia Moreton[1], David Ferreira[1], Malcolm Roberts[2], Helene Hewitt[2]

[1]University of Reading, UK
[2]UK Met Office Hadley Centre, Exeter, UK

Key Points:

- Global turbulent heat flux feedback over coherent mesoscale eddies ranges between 35-45 W m^{-2} K^{-1}
- Ocean to atmosphere SST regridding can underestimate turbulent heat flux feedback by up to 75%
- Coupled models need a coordinated increase in ocean and atmosphere resolutions

Corresponding author: Sophia Moreton, `s.moreton@pgr.reading.ac.uk`

Abstract

Air-sea turbulent heat fluxes play a fundamental role in generating and dampening sea surface temperature (SST) anomalies. To date, the turbulent heat flux feedback (THFF) is well quantified at basin-wide scales (~20 W m^{-2} K^{-1}) but remains unknown at the oceanic mesoscale (10-100 km). Here, using an eddy-tracking algorithm in three configurations of the coupled climate model HadGEM3-GC3.1, the THFF over mesoscale eddies is estimated. The THFF magnitude is strongly dependent on the ocean-to-atmosphere regridding of SST, a common practice in coupled models for calculating air-sea heat flux. Our best estimate shows that the mesoscale THFF ranges between 35 and 45 W m^{-2} K^{-1} globally, across different eddy amplitudes. Increasing the ratio of atmosphere-to-ocean grid resolution can lead to an underestimation of the THFF, by as much as 75% for a 6:1 resolution ratio. Our results suggest that a large atmosphere-to-ocean grid ratio can result in an artificially weak dampening of mesoscale SST anomalies.

Plain language summary: Sea surface temperature (SST) anomalies are vital for both regulating the earth's weather and climate. The generation and reduction of these SST anomalies is largely determined by air-sea heat fluxes, particularly turbulent (latent and sensible) heat fluxes. So far in current research, the feedback from these turbulent heat fluxes is well known at large scales, i.e. over the whole ocean basin. However, a quantification of this feedback at much smaller spatial scales (10-100 km) over individual mesoscale ocean eddies is still missing. Due to the availability of high resolution data from a coupled climate model, this study provides the first global estimate of this feedback over individually tracked and averaged mesoscale eddies. The estimate ranges between 35 to 45 W m^{-2} K^{-1}, depending on an eddy's sea surface height anomaly. In coupled climate models, if the spatial resolution of the atmospheric grid is much larger than the ocean grid resolution, with a ratio 6:1, a 75% underestimation of this feedback occurs. This massive underestimation suggests, in this model, SST anomalies within mesoscale eddies are not reduced enough by air-sea heat fluxes, and consequently will remain too large.

1 Introduction

The turbulent heat flux feedback (THFF, in W m^{-2} K^{-1}, denoted α hereafter) is a critical parameter, which measures the change in the net air-sea turbulent heat flux in response to a 1 K change in sea surface temperature (SST). It is a powerful tool to quantify the rate of dampening of SST anomalies. THFF can vary seasonally (largest in winter), geographically and with ocean spatial scale. Early studies estimate THFF at approximately 20 W m^{-2} K^{-1} for basin-scale mid-latitude SST anomalies, which, to first order, respond passively to atmospheric forcing (Bretherton, 1982; Frankignoul, 1985; Frankignoul, Czaja, & L'Heveder, 1998; Frankignoul et al., 2004; Small, Bryan, Bishop, Larson, & Tomas, 2020). More recent studies estimate that THFF increases to 40 W m^{-2} K^{-1} in the Gulf Stream, and decreases down to 10 W m^{-2} K^{-1} in the Antarctic Circumpolar Current (Hausmann & Czaja, 2012; Hausmann, Czaja, & Marshall, 2017). To date, while THFF is known to increase towards smaller scales, the smallest spatial scale used to quantify THFF is approximately 100 km.

The magnitude of THFF depends on the background SST and the adjustment of the atmospheric boundary layer (ABL) to the SST anomaly. It is suggested that the removal of heat by surface winds is a key process (Bretherton, 1982; Hausmann, Czaja, & Marshall, 2016). On smaller scales, heat can easily be advected away from the SST anomaly, maintaining a large air-sea temperature contrast and strong heat flux damping. While on basin scales, this process becomes less efficient (slower), resulting in a small temperature contrast and large damping. On global scale, this adjustment completely disappears: the heat removal is controlled by radiation out to space and the THFF reaches only about 1-2 W m^{-2} K^{-1} (Gregory et al., 2004). However, how the THFF behaves at spatial scales below 100 km remains unknown.

Formed through intrinsic ocean variability, mesoscale eddy SST anomalies (of radius 10-100 km) drive distinct changes within the ABL through the so-called 'vertical mixing mechanism' (Frenger, Gruber, Knutti, & Münnich, 2013; Hayes, McPhaden, & Wallace, 1989; Putrasahan, Miller, & Seo, 2013; Small, Bryan, Bishop, & Tomas, 2019; Wallace, Mitchell, & Deser, 1989). A warm mesoscale SST anomaly transfers heat through turbulent heat fluxes up into the ABL, which increases local vertical mixing, reduces stability and extends the height of the ABL. The increase in mixing encourages the transfer of momentum downwards and strengthens surface winds, cloud cover and rainfall. The opposite occurs over a cold SST anomaly. Past research on mesoscale air-sea exchanges largely focuses on momentum fluxes however in eddy-rich regions, mesoscale-induced air-sea turbulent heat fluxes play an important role in altering eddy kinetic and potential energy and dampening SST anomalies (Bishop, Small, & Bryan, 2020; Hogg, Dewar, Berloff, Kravtsov, & Hutchinson, 2009; Renault, Marchesiello, Masson, & McWilliams, 2019; Renault et al., 2016; Seo, Miller, & Norris, 2016). Furthermore, mesoscale SST-turbulent heat flux exchanges can strengthen western boundary currents (WBC) by 20 to 40% and weaken thermal stratification in the upper ocean (Ma et al., 2016; Shan et al., 2020; Small et al., 2020). It is therefore important to provide a quantification of THFF over transient mesoscale eddies.

Observational estimates of THFF at the oceanic mesoscale are restricted by the availability of high-resolution ocean and atmosphere data. First, the consistency and effective resolution of global air-sea heat flux datasets are questionable, due to the different space-time resolutions from either atmospheric reanalysis or satellites (Cronin et al., 2019; Leyba, Saraceno, & Solman, 2016; Li, Sang, & Jing, 2017; Villas Bôas, Sato, Chaigneau, & Castelão, 2015). Second, radii of mesoscale eddies, estimated from gridded sea surface height product such as AVISO [Archiving, Validation and Interpolating of Satellite Oceanographic Data, 2014] maybe be overestimated by a factor of 2 due to the interpolation of raw satellite tracks needed to create a gridded product (Chelton, 2013; Cronin et al., 2019; Ducet, Le Traon, & Reverdin, 2000; Hausmann & Czaja, 2012; Minobe, Kuwano-Yoshida, Komori, Xie, & Small, 2008; Moreton, Ferreira, Roberts, & Hewitt, 2020; Small et al., 2008; Xie, 2004). As a result, this study uses a global coupled climate model with higher spatial ocean and atmospheric resolution than currently available in observations.

Current state-of-the-art climate models can provide global eddy-rich ocean simulations, with a horizontal resolution of approximately 1/12°. At this resolution, mesoscale eddies can be explicitly resolved globally, except in the highest latitudes with more, smaller and longer-lasting eddies compared to a 1/4° resolution (Haarsma et al., 2016; Hewitt et al., 2017; Moreton et al., 2020; M. J. Roberts et al., 2019). However, whether an eddy-rich ocean results in an improved representation of mesoscale SST-turbulent heat flux exchanges remains to be determined. The ratio of ocean-atmosphere horizontal resolution is likely to be an important factor (Jullien et al., 2020). In many current high-resolution coupled models, with the exception of the Community Earth System Model (CESM), air-sea fluxes are computed on the atmospheric grid, which requires the interpolation of SST from the oceanic grid to the often coarser atmospheric grid (Yang, Jing, & Wu, 2018). The interpolation is likely to smooth out mesoscale features resolved on the ocean grid before calculation of the air-sea exchanges and if so, to introduce significant biases in air-sea feedbacks.

Therefore, the following study has two goals: 1) to provide the first estimate of THFF over coherent mesoscale eddies globally at smaller spatial scales than previously evaluated and 2), to evaluate if THFF is dependent on the ratio of ocean-atmosphere resolution in coupled models. The three configurations of a high-resolution coupled climate model, and the methods to compute and rationalize THFF at the mesoscale are introduced in section 2. Section 3 presents the results addressing the two goals, and finally section 4 concludes and discusses implications for future research and model development.

2 Materials and Methods

2.1 Model data

The following results use output from the high-resolution global coupled climate model, HadGEM3-GC3.1 (Williams et al., 2018). The climate model couples an atmosphere (MetUM), land (JULES), ocean (NEMO) and sea ice (CICE) components (Madec, 2008; Storkey et al., 2018; Walters et al., 2017). The model simulations follow the CMIP6 HighResMIP protocol, as part of PRIMAVERA (Haarsma et al., 2016; M. J. Roberts et al., 2019). Three configurations of this model are compared, with a different ratio of ocean-atmosphere resolution: N512-12 ($\sim$25 km atmosphere, 1/12° ocean), N216-12 ($\sim$60 km atmosphere, 1/12° ocean) and finally, N216-025 ($\sim$60 km atmosphere, 1/4° ocean). Model outputs are obtained after a 20-year spin-up, and one year of daily data is used (the results are independent of the year chosen).

To compute air-sea turbulent (latent and sensible) heat fluxes (THFs), the OASIS3 coupler passes the ocean model SST to the atmospheric grid using a second-order conservative interpolation (Hewitt et al., 2011; Valcke, 2013; Valcke, Craig, & L., 2015). In the following, the SST on the ocean grid (SST_O) is distinguished from the regridded SST on the atmospheric grid (SST_A). Positive values of THF denote fluxes upwards from the ocean to the atmosphere. Finally, surface air temperature is taken at 1.5 m.

2.2 Eddy tracking and compositing

Closed coherent mesoscale eddies are identified and tracked daily in the global ocean for 20 years from sea surface height (SSH), using an eddy tracking algorithm. The algorithm is adapted from Mason, Pascual, and McWilliams (2014) and Chelton, Schlax, and Samelson (2011). As well as being dependent on SSH contours, an eddy is tracked subject to certain criteria, such as a shape test or pixel number. The algorithm is described in detail in Moreton et al. (2020). A discussion of the eddy characteristics and comparison of the model with the AVISO satellite product is also provided by Moreton et al. (2020).

To isolate mesoscale anomalies, a 10-year climatological mean is removed from the fields which are subsequently high-pass filtered (using the same filter as for eddy tracking, see SPM for details). Following Frenger et al. (2013); Hausmann and Czaja (2012); Villas Bôas et al. (2015), 'composite averaging' is used to remove high-frequency variability associated with weather (shown in Fig. 1 from N512-12), as follows. High-pass filtered anomalies centered on each eddy are normalized by the effective eddy radius (L_{eff}) and averaged for all eddies globally. L_{eff} is defined as the radius of a fitted circle with

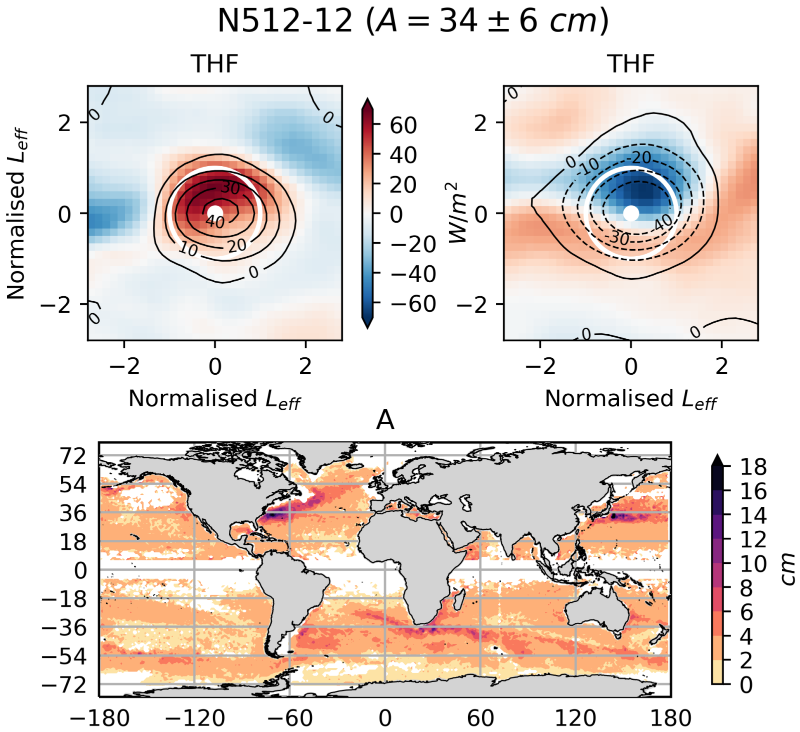

Figure 1. Composite maps of turbulent heat flux THF (colour shading, in W m^{-2}) and SSH (black lines, in cm) for large-amplitude (A=34±6 cm) anti-cyclonic (upper left) and cyclonic (upper right) eddies from N512-12. Solid (dashed) lines indicate positive (negative) values. The white dot is the centre of each tracked eddy and the white circle is 1 effective eddy radius (L_{eff}). (bottom panel) The map is eddy amplitude (A, in cm) binned into a 1° grid from the tracked eddies in N512-12.

the same area as the outermost closed SSH contour in each tracked eddy. Composites are plotted in units of L_{eff}. Rotating the anomalies (to align with background SST or wind direction) before averaging was found to make little difference to the results.

Finally, the eddies and their associated fields are binned according to their eddy amplitude (A) from 1±0.05 cm to 34±6 cm. A global map of the averaged eddy amplitude per 1° squared is shown in Fig. 1. As expected, larger amplitude eddies are concentrated in eddy-rich regions, such as WBCs and the Southern Ocean. A is the absolute difference between either the maximum (for anti-cyclones) or minimum (cyclones) SSH and the SSH magnitude at the outermost closed SSH contour of the tracked eddy. This means the SSH anomaly is larger than eddy amplitude and can extend spatially beyond the tracked eddy radius (Fig. 1). It should be highlighted that eddy amplitude and eddy radius are not strongly related (Chelton et al., 2011; Moreton et al., 2020). Instead, eddy amplitude is linearly related to SST anomalies, especially for $A \leq$25 cm, shown in SPM Fig. S3 B,C, as found in previous studies (Villas Bôas et al., 2015).

An accurate comparison of eddy composites from the model to observations is difficult, due to the coarser resolution found in observations and differences in either how the SSH anomalies are isolated (i.e. by standard deviation of SSHA or eddy tracking), the eddy tracking algorithm or in the strength of the high-pass filtering. However, the SST_O composites in the model (maximum of 0.5-0.6 K using binned eddy amplitudes of 15 cm) and in a previous observational study (0.7 K) have similar magnitudes and spatial distributions, i.e. a monopole for larger amplitude or a dipole for smaller amplitude eddies (Hausmann & Czaja, 2012). Larger differences between the model and observations are found for LHF anomalies, especially at larger amplitudes (20-30 cm): N512-12 has a maximum LHF anomaly of 32 W m^{-2} K^{-1}, whilst only 5-7 W m^{-2} K^{-1} in observations (Villas Bôas et al., 2015).

2.3 Decomposition of the turbulent heat flux feedback

The THFF α is defined as:

$$< THF' >= \alpha < SST' > \tag{1}$$

where primes indicate the high-pass filtered anomalies, and $< . >$ indicates the composite averaging over all eddies. A positive value of α represents a negative heat flux feedback, i.e. a dampening of the SST anomaly by turbulent heat fluxes.

Due to the regridding of SST to calculate air-sea heat fluxes in the coupled model, two THFFs can be computed from either SST_A or SST_O:

$$< THF' > \; = \; \alpha_O < SST'_O > \tag{2}$$

$$< THF' > \; = \; \alpha_A < SST'_A > . \tag{3}$$

The THFF α_O relates the THF anomalies to the prognostic SST anomalies in the ocean component, while α_A represents the THFF after re-gridding the ocean grid SST to the atmospheric grid (SST_A). Note that α_A does not affect directly the prognostic state of the simulation. By isolating THFF based on SST_O (α_O) or based on re-gridded SST (α_A), we can provide an estimate for how the THFF is affected by the ratio of ocean-atmosphere resolution in coupled models.

To understand the behaviour of the THFFs α_O and α_A, it is useful to introduce three coefficients λ_A, δ and R_g (Eqs. 4-6 below). First, the THF restoring coefficient λ_A is a simplification of the latent and sensible heat flux (LHF and SHF) bulk formulae used in the model (Large & Yeager, 2004). Following Frankignoul et al. (1998) and Hausmann et al. (2017)), we assume that the LHF can be linearized to be expressed in terms of the air-sea temperature difference, $T_{air} - SST_A$. Second, δ measures the adjustment of the surface air temperature T_{air} to the regridded SST anomalies SST_A: when δ equals zero there is no ABL response or adjustment, whilst when δ equals one, a complete adjustment occurs resulting in a zero THF. Third, the R_g coefficient measures the impact of the ocean-to-atmosphere regridding on the SST magnitude. If R_g equals one, the magnitude of the SST anomalies is preserved during the regridding.

$$
\begin{aligned}
< THF' > &= \lambda_A(< SST'_A > - < T'_{air} >) &(4)\\
< T'_{air} > &= \delta < SST'_A > &(5)\\
< SST'_A > &= R_g < SST'_O > . &(6)
\end{aligned}
$$

By re-arranging, relationships between the coefficients can be derived, in order to trace changes from the THF restoring coefficient λ_A to α_O:

$$
\begin{aligned}
\alpha_A &= (1-\delta)\ \lambda_A &(7)\\
\alpha_O &= R_g\ \alpha_A &(8)
\end{aligned}
$$

The THFF α_A is scaled down from λ_A by the air temperature adjustment in the ABL (Eq. 7). When the ABL temperature adjustment is weak (i.e. $\delta \sim 0$), α_A is close to the restoring embedded in the THF bulk formulae (i.e. λ_A here). Whilst when the adjustment is strong, the THFF α_A, and subsequently the dampening of SST anomalies, is much smaller than predicted by λ_A (Frankignoul et al., 1998). In other words, the coefficient λ_A represents an upper bound for α_A, which is achieved when air temperature adjustment (δ) is zero. This upper bound is the "fast limit" discussed by Hausmann et al. (2017).

The THFF using ocean model SST (α_O) is reduced from α_a by the SST regridding coefficient R_g (Eq. 8). It is anticipated that R_g is smaller than one and therefore α_O is biased low compared to α_A.

In practice, the above coefficients are estimated over coherent mesoscale eddies through a linear regression between the points of the composite maps (see Fig. 2). Since SST, T_{air} and THF anomalies tend to extend outside the eddy radius, points up to ± 2.8 times the eddy radius are included in the linear regression. Regressions for anti-cyclonic and cyclonic eddies are calculated separately, and a weighted average is used to produce a total value (given as text in Fig. 2). The gradients of linear regression are dependent on $SST_{O/A}$ being on the $x - axis$.

3 Results

First the THFF coefficients, α_A and α_O, are discussed for the N512-12 configuration, which is the least affected by regridding biases (section 3.1). A comparison to N216-12 and N216-025 configurations follows, to evaluate the impact of changes in the ratio of ocean-atmosphere resolutions on the THFF (section 3.2).

3.1 Estimating THFF over large-amplitude mesoscale eddies

Fig. 2 illustrates the relationships between the composite fields for the large amplitude eddies (A=34±6 cm) globally in N512-12. A repeat of the relationships for small-amplitude mesoscale eddies (A=1±0.05 cm) can be found in the Appendix (Fig. S1). The estimated coefficients $\alpha_{O/A}$, λ_A, δ and R_g from Eqs. (2)-(6) are indicated in each panel with error bars.

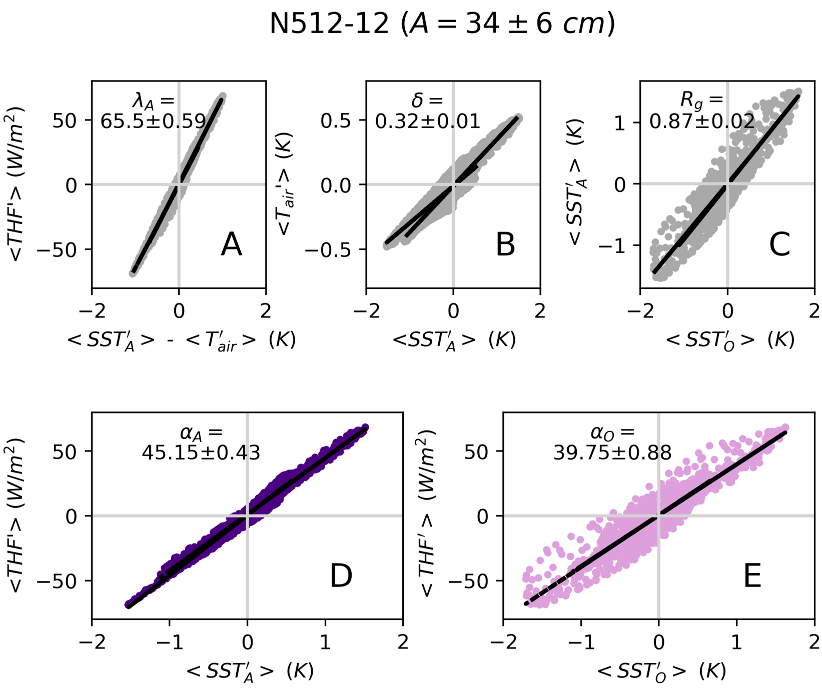

Figure 2. Relationships between the composite fields of $SST_{O/A}$, THF and T_{air}, with the estimated coefficients ($\alpha_{O/A}$, λ_A, δ and R_g) for the larger amplitude eddies (A=34±6 cm) globally in N512-12. The coefficients are given by gradient of the linear regression line (black) +/- the 95% confidence interval.

There is a strong linear relationship between the composite anomalies of THF and air-sea temperature contrast (Fig. 2A), providing a robust estimate of λ_A at 65.5±0.59 W m^{-2} K^{-1}.

This is larger than previous estimates of about 50 W m^{-2} K^{-1} (Frankignoul et al., 1998; Rahmstorf & Willebrand, 1995) and the upper bound of 25-35 W m^{-2} K^{-1} of Hausmann et al. (2017). This discrepancy could reflect differences in the estimation methods. Published estimates are based on the linearization of bulk formulae using constant drag coefficients and monthly-mean large-scale winds. In contrast, our estimates (Fig. 2A) implicitly account for 1) the full complexity of the bulk formulae implemented in HadGEM3-GC3.1, where the drag coefficient is function of ABL stability and surface winds (Hewitt et al., 2011) and 2) dynamical adjustments in the ABL such as the modulation of surface winds by mesoscale eddy SST anomalies (Frenger et al., 2013; M. J. Roberts et al., 2016).

The atmospheric adjustment parameter δ is estimated at 0.32$\pm$0.01 for large amplitude eddies globally (Fig. 2B), i.e. the surface air temperature T_{air} anomaly is about a third of the mesoscale SST anomaly. Previous studies give 0.5 in the WBCs and the Antarctic Circumpolar Current (ACC) core, increasing to 0.9 in quiescent regions (Hausmann et al., 2017). However, these estimates are limited by the scale of ERA-I reanalysis (0.75$\times$0.75°) and do not isolate coherent eddies. Although the modelled large-amplitude eddies used in Fig. 2 are mostly found in WBCs (Fig. 1), our estimate suggests that T_{air} adjustments drop further below 0.5 over coherent mesoscale eddies.

The value of α_A ($\sim$45 W m^{-2} K^{-1}, Fig. 2D) can now be explained by combining estimates of λ_A and δ using Eq. (7): $\alpha_A \simeq (1 - 0.32) \times 65.5 \simeq 45$ W m^{-2} K^{-1} . As most large-amplitude eddies are found in the WBCs, our modelled estimate of α_A agrees well with previous observational estimates of 40-56 W m^{-2} K^{-1} in the Kuroshio region and 40 W m^{-2} K^{-1} in the Gulf Stream (Hausmann et al., 2016; Ma et al., 2015). Finally, the THFF on the prognostic SST, α_O, is about 10% smaller than α_A at about 40 W m^{-2} K^{-1} (Fig. 2E). The reduction reflects the 10% decrease in the amplitude of mesoscale SST anomalies brought by the SST regridding ($R_g \simeq 0.9$, see Eq. (8); Fig. 2C).

Fig. 3A presents variations of α_A and α_O as a function of eddy amplitude A in N512-12. To first order, the THFF increases with eddy amplitude (and hence SST anomalies, see Fig. S1). From a minimum of $\sim$34 W m^{-2} K^{-1} at 5$\pm$0.05 cm, α_A increases to 40-45 W m^{-2} K^{-1} at 34$\pm$6 cm and to $\sim$40 W m^{-2} K^{-1} on the smallest amplitudes (1-3$\pm$0.05 cm). Referring to Eq. (7), variations in α_A are mainly driven by changes in the THF restoring λ_A whilst the atmospheric adjustment δ is relatively insensitive to eddy amplitude (compare Fig. S3 D and E). Variations in α_O follow those of α_A except at the smallest amplitudes where R_g decreases from 0.9 to about 0.7 (Fig 3D in purple for N512-12).

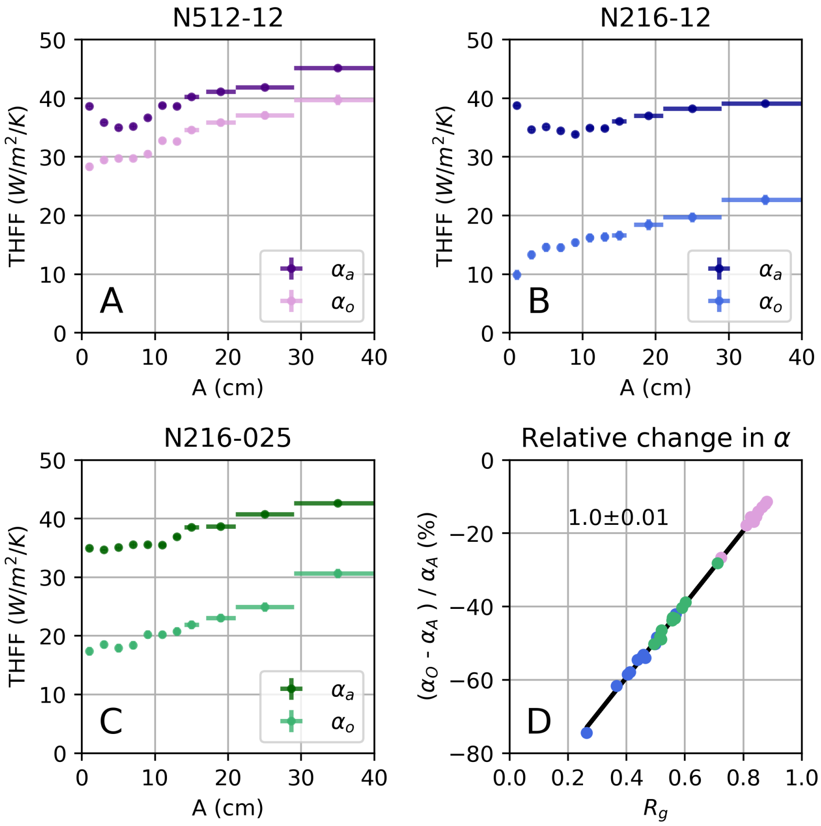

Figure 3. THFF α_A and α_O as a function of the eddy amplitude (in cm) for N512-12 (subplot A), N216-12 (B) and N216-025 (C), as indicated in the titles. The horizontal bars indicate the width of the eddy amplitude bins, and the vertical error bars indicate 95% confidence intervals. The relative change between α_O and α_A (in %) (subplot D) is shown as a function of R_g for all eddy amplitudes and all model configurations. The gradient of the linear regression line is added as text, to be compared with the theoretical slope of 1 – see Eq. (8).

3.2 Impact of the ratio of ocean-atmosphere resolution on THFF

Fig. 3 summarizes estimates of α_A and α_O for all configurations and eddy amplitudes. Variations of α_A are very similar across configurations. This is not surprising as α_A depends on quantities evaluated on the atmospheric grid: the bulk formulae through λ_A (which are the same in all configurations) and the atmospheric adjustment δ which directly 'feels' SST_A (Eq. 7). In contrast, α_O varies greatly depending on the mismatch between grid resolutions in ocean and atmosphere. α_O is biased low relative to α_A by about 5, 15, and 20 W m^{-2} K^{-1} in N512-12, N216-025 and N216-12, respectively. In N216-12, the low bias increases to 25-30 W m^{-2} K^{-1} for the small amplitude eddies (<5 cm).

Across all configurations and eddy amplitudes, the relative change between α_O and α_A exhibits a strong linear correlation with the regridding parameter R_g, with a slope of 1 as expected from Eq. (8) (Fig. 3D). This reinforces our interpretation that the regridding of SST (captured by R_g) plays a fundamental role in determining α_O's low biases. The difference between α_O and α_A increases with R_g from -15-20% for N512-12, to -40-50% for N216-025 and to -50-75% for N216-12. Crucially, the low bias is the largest for the smaller amplitude eddies, which cover most of the global ocean, in the configuration with the largest ratio between atmospheric and oceanic resolutions: N216-12. For the small amplitude eddies in N216-12, eddy spatial scale (L_{eff} ∼40 km) is smaller than the atmospheric grid-scale (∼60 km). However in N512-12, the scale of small amplitude eddies (L_{eff} ∼40 km) is larger than the atmospheric grid-scale (∼25 km), resulting in a minimal distortion from SST_O to SST_A (Fig. 3A). Regridding of SST_O reduces the amplitude of the mesoscale SST anomalies and creates a spatial shift between SST_O and SST_A (Fig. S). As the heat fluxes are computed from SST_A, this creates a spatial mismatch between the heat flux damping and the prognostic SST, SST_O.

4 Conclusions

Turbulent heat flux feedbacks over coherent mesoscale eddies are estimated globally in three configurations of a high-resolution coupled model HadGEM3-GC3.1. First, for the highest ocean-atmosphere resolution available (where the impact of SST regridding from the ocean grid to the atmosphere grid is minimal), the modelled estimates of the THFF over mesoscale eddies are approximately 35-45 W m^{-2} K^{-1} depending on eddy amplitude. This is the first time this estimate has been provided as previous studies did not resolve such small scales nor attempted to isolate coherent eddies. Second, we investigate configurations with larger mismatch between oceanic and atmospheric resolutions. We find that the regridding of SST from the ocean to atmosphere grid results in an underestimate of the eddy-induced THFF ranging from 10 to 75%. Importantly, this low bias increases with the ratio between atmospheric and ocean resolutions, implying that increasing the oceanic resolution at constant atmospheric resolution can actually degrade the solution, at least in the representation of air-sea feedbacks.

The low bias in the α_O feedback suggests that eddy SST anomalies are not dampened enough in the model. The importance of correctly simulating the THFF over mesoscale eddies is fundamental in order to represent realistic mesoscale SST anomalies within eddies and to replicate their interaction with the local and large-scale atmosphere, as well as the feedback onto the eddy itself. Even small-amplitude (∼1 cm) eddies found across the open ocean have a strong THFF between 35-40 W m^{-2} K^{-1} emphasising the importance of transient eddies outside the eddy-rich WBCs and the ACC. Although eddy-induced THFF can influence the upper-ocean heat budget and weaken thermal stratification (Shan et al., 2020), further work is needed to understand its impact on large-scale ocean circulation, and its feedback on eddy lifetime.

There is considerable variation (up to 40%) between different simulations of mesoscale air-sea exchanges in high-resolution coupled models and our study is limited to one model (Yang et al., 2018). Note that the time evolution of the atmospheric adjustment is not explored, which is likely to affect the THFF strength (Frankignoul et al., 1998; Hausmann et al., 2017). Finally, this study focuses on horizontal resolution but changes in the vertical resolution, in both the ocean and atmosphere, is likely to impact the representation of mesoscale eddy-induced SST anomalies and overlying atmospheric adjustment.

The results in this study hold implications for future model development. Similarly to HadGEM3-GC3.1, many current high-resolution coupled models (e.g. HighResMIP) compute air-sea turbulent heat fluxes on the atmospheric grid, using regridded SST (M. J. Roberts et al., 2019; Valcke et al., 2015). For the long spin-ups needed for climate simulations, it is unrealistic to expect the atmospheric resolution to match the oceanic resolution. Instead, it is advised when fully resolving mesoscale air-sea exchanges, that air-sea heat fluxes should be calculated on the finer-scale oceanic grid, as done by the Community Earth System Model (see Yang et al. (2018)). This method ensures at least that the high-resolution SST anomalies are maintained. In ocean-only models, the ocean component is driven through bulk formulae and prescribed surface atmospheric fields, i.e. without ABL adjustment (i.e. $\delta = 0$). In such setups, we expect mesoscale THFF to approach λ_A. However, the absence of an ABL adjustment also influences λ_A (e.g. neglecting the effect of dynamical adjustment on the drag coefficient). The net effect of these assumptions on the mesoscale THFF in ocean-only models remains to be quantified.

Acknowledgments

S. Moreton is funded by the NERC CASE Studentship, UK (NE/N008448/1) and the Met Office CASE studentship, UK. Met Office authors were supported by the Joint UK BEIS/Defra Met Office Hadley Centre Climate Programme (GA01101). M. Roberts acknowledges funding received from the European Commission under Grant Agreement 641727 (PRIMAVERA project) of the Horizon 2020 research programme. There are no conflicts of interest for the authors.

5 Data Availability statement

HighResMIP model data used in this study is freely available from the Earth System Grid Federation (ESGF), https://esgf-index1.ceda.ac.uk/search/primavera-ceda/. The N512-12 configuration datasets (HadGEM3-GC31-HH) are available here: M. Roberts (2018). The N216-12 configuration datasets (HadGEM3-GC31-MH) are available here: M. Roberts (2017a). The N216-025 configuration datasets (HadGEM3-GC31-MM) are available here: M. Roberts (2017b). A dataset of the tracked mesoscale eddies (and their properties) is freely available here (Moreton & Roberts, 2021) in a repository, under a Creative Commons Attribution 4.0 International Licence: https://creativecommons.org/licenses/by/4.0/. The 1-yr of data chosen for this study is given in the supplemental material.

References

Bishop, S. P., Small, R. J., & Bryan, F. O. (2020). The Global Sink of Available Potential Energy by Mesoscale Air-Sea Interaction. *Journal of Advances in Modeling Earth Systems*. doi: 10.1029/2020ms002118

Bretherton, F. P. (1982). Ocean climate modeling. *Progress in Oceanography*, *11*(2), 93–129. doi: 10.1016/0079-6611(82)90005-2

Chelton, D. B. (2013). Ocean–atmosphere coupling: Mesoscale eddy effects. *Nature Geoscience*, *6*(8), 594–595. Retrieved from `http://www.nature.com/doifinder/10.1038/ngeo1906` doi: 10.1038/ngeo1906

Chelton, D. B., Schlax, M. G., & Samelson, R. M. (2011). Global observations of nonlinear mesoscale eddies. *Progress in Oceanography*, *91*, 167 – 216. doi: 10.1016/j.pocean.2011.01.002

Cronin, M. F., Gentemann, C. L., Edson, J., Ueki, I., Bourassa, M., Brown, S., ... Zhang, D. (2019). Air-Sea Fluxes With a Focus on Heat and Momentum. *Frontiers in Marine Science*, *6*(July). doi: 10.3389/fmars.2019.00430

Ducet, N., Le Traon, P. Y., & Reverdin, G. (2000). Global high-resolution mapping of ocean circulation from TOPEX/Poseidon and ERS-1 and -2. *Journal of Geophysical Research: Oceans*, *105*(C8), 19477–19498. doi: 10.1029/2000jc900063

Frankignoul, C. (1985). Sea Surface Temperature Anomalies, Planetary Waves,. *Reviews of Geophysics*, *23*(4), 357–390.

Frankignoul, C., Czaja, A., & L'Heveder, B. (1998). Air-sea feedback in the North Atlantic and surface boundary conditions for ocean models. *Journal of Climate*, *11*(9), 2310–2324. doi: 10.1175/1520-0442(1998)011⟨2310:ASFITN⟩2.0.CO;2

Frankignoul, C., Kestenare, E., Botzet, M., Carril, A. F., Drange, H., Pardaens, A., ... Sutton, R. (2004). An intercomparison between the surface heat flux feedback in five coupled models, COADS and the NCEP reanalysis. *Climate Dynamics*, *22*(4), 373–388. doi: 10.1007/s00382-003-0388-3

Frenger, I., Gruber, N., Knutti, R., & Münnich, M. (2013). Imprint of Southern Ocean eddies on winds, clouds and rainfall. *Nature Geoscience Letters*, *6*, 608 – 612. doi: 10.1038/NGEO1863

Gregory, J. M., Ingram, W. J., Palmer, M. A., Jones, G. S., Stott, P. A., Thorpe, R. B., ... Williams, K. D. (2004). A new method for diagnosing radiative forcing and climate sensitivity. *Geophysical Research Letters*, *31*(3), 2–5. doi: 10.1029/2003GL018747

Haarsma, R. J., Roberts, M. J., Vidale, P. L., Catherine, A., Bellucci, A., Bao, Q.,

... Von Storch, J. S. (2016). High Resolution Model Intercomparison Project (HighResMIP v1.0) for CMIP6. *Geoscientific Model Development*, *9*(11), 4185–4208. doi: 10.5194/gmd-9-4185-2016

Hausmann, U., & Czaja, A. (2012). The observed signature of mesoscale eddies in sea surface temperature and the associated heat transport. *Deep-Sea Research Part I: Oceanographic Research Papers*, *70*, 60–72. Retrieved from `http://dx.doi.org/10.1016/j.dsr.2012.08.005` doi: 10.1016/j.dsr.2012.08.005

Hausmann, U., Czaja, A., & Marshall, J. (2016). Estimates of air-sea feedbacks on sea surface temperature anomalies in the Southern Ocean. *Journal of Climate*, *29*(2), 439–454. doi: 10.1175/JCLI-D-15-0015.1

Hausmann, U., Czaja, A., & Marshall, J. (2017). Mechanisms controlling the SST air-sea heat flux feedback and its dependence on spatial scale. *Climate Dynamics*, *48*(3-4), 1297–1307. doi: 10.1007/s00382-016-3142-3

Hayes, S. P., McPhaden, M. J., & Wallace, J. M. (1989). The influence of Sea Surface Temperature on Surface Wind in the Eastern Equatorial Pacific: Weekly to Monthly Variability. *Journal of Climate*, *2*, 1500–1506.

Hewitt, H. T., Bell, M. J., Chassignet, E. P., Czaja, A., Ferreira, D., Griffies, S. M., ... Roberts, M. J. (2017). *Will high-resolution global ocean models benefit coupled predictions on short-range to climate timescales?* (Vol. 120). doi: 10.1016/j.ocemod.2017.11.002

Hewitt, H. T., Copsey, D., Culverwell, I. D., Harris, C. M., Hill, R. S., Keen, A. B., ... Hunke, E. C. (2011). Design and implementation of the infrastructure of HadGEM3: The next-generation Met Office climate modelling system. *Geoscientific Model Development*, *4*(2), 223–253. doi: 10.5194/gmd-4-223-2011

Hogg, A. M., Dewar, W. K., Berloff, P., Kravtsov, S., & Hutchinson, D. K. (2009). The effects of mesoscale ocean-atmosphere coupling on the large-scale ocean circulation. *Journal of Climate*. doi: 10.1175/2009JCLI2629.1

Jullien, S., Masson, S., Oerder, V., Samson, G., Colas, F., & Renault, L. (2020). Impact of ocean-atmosphere current feedback on ocean mesoscale activity: Regional variations and sensitivity to model resolution. *Journal of Climate*, *33*(7), 2585–2602. doi: 10.1175/JCLI-D-19-0484.1

Large, W., & Yeager, S. (2004). Diurnal to Decadal Global Forcing The Data Sets and Flux Climatologies. *NCAR Tech. Note*(2004), 1–105. doi: 10.5065/D6KK98Q6

Leyba, I. M., Saraceno, M., & Solman, S. A. (2016). Air-sea heat fluxes associated to mesoscale eddies in the Southwestern Atlantic Ocean and their dependence on different regional conditions. *Climate Dynamics*, *49*(7-8), 2491–2501. doi:

10.1007/s00382-016-3460-5

Li, F., Sang, H., & Jing, Z. (2017). Quantify the continuous dependence of SST-turbulent heat flux relationship on spatial scales. *Geophysical Research Letters*, *44*(12), 6326–6333. doi: 10.1002/2017GL073695

Ma, X., Chang, P., Saravanan, R., Montuoro, R., Hsieh, J., Wu, D., … Jing, Z. (2015). Distant Influence of Kuroshio Eddies on North Pacific Weather Patterns ? *Nature: Scientific Reports*.

Ma, X., Jing, Z., Chang, P., Liu, X., Montuoro, R., Small, R. J., … Wu, L. (2016). Western boundary currents regulated by interaction between ocean eddies and the atmosphere. *Nature*, *535*(7613), 533–537. Retrieved from `http://www.nature.com/doifinder/10.1038/nature18640` doi: 10.1038/nature18640

Madec, G. (2008). NEMO ocean engine. *Note du Pôle de modélisation, Institut Pierre-Simon Laplace (IPSL), France*(27), 1 – 396.

Mason, E., Pascual, A., & McWilliams, J. C. (2014). A new sea surface height-based code for oceanic mesoscale eddy tracking. *Journal of Atmospheric and Oceanic Technology*, *31*(5), 1181–1188. doi: 10.1175/JTECH-D-14-00019.1

Minobe, S., Kuwano-Yoshida, A., Komori, N., Xie, S. P., & Small, R. J. (2008). Influence of the Gulf Stream on the troposphere. *Nature*, *452*(7184), 206–209. doi: 10.1038/nature06690

Moreton, S. M., Ferreira, D., Roberts, M., & Hewitt, H. (2020). Evaluating surface eddy properties in coupled climate simulations with 'eddy-present' and 'eddy-rich' ocean resolution. *Ocean Modelling*, *147*. doi: 10.1016/j.ocemod.2020.101567

Moreton, S. M., & Roberts, M. (2021). *An eddy tracking dataset for N512-12, N216-12 and N216-025 model configurations of HadGEM3-GC3.1 .* Retrieved from `https://researchdata.reading.ac.uk/id/eprint/283` doi: http://dx.doi.org/10.17864/1947.283.

Putrasahan, D. A., Miller, A. J., & Seo, H. (2013). Isolating mesoscale coupled ocean-atmosphere interactions in the Kuroshio Extension region. *Dynamics of Atmospheres and Oceans*, *63*, 60–78. Retrieved from `http://dx.doi.org/10.1016/j.dynatmoce.2013.04.001` doi: 10.1016/j.dynatmoce.2013.04.001

Rahmstorf, S., & Willebrand, J. (1995). The Role of Temperature Feedback in Stabilizing the Thermocline Circulation. *Journal of Physical Oceanography*, *25*, 787–805.

Renault, L., Marchesiello, P., Masson, S., & McWilliams, J. C. (2019). Remarkable Control of Western Boundary Currents by Eddy Killing, a Mechanical Air-

Sea Coupling Process. *Geophysical Research Letters*, *46*(5), 2743–2751. doi: 10.1029/2018GL081211

Renault, L., Molemaker, M. J., McWilliams, J. C., Shchepetkin, A. F., Lemarié, F., Chelton, D. B., ... Hall, A. (2016). Modulation of Wind-Work by Oceanic Current Interaction with the Atmosphere. *Journal of Climate*, *46*, 1685 – 1703. doi: 10.1175/JPO-D-15-0232.1

Roberts, M. (2017a). *MOHC HadGEM3-GC31-MH model output prepared for CMIP6 HighResMIP. Version 20190901.* Retrieved from `http://doi.org/10.22033/ESGF/CMIP6.1762` doi: http://doi.org/10.22033/ESGF/CMIP6.1762

Roberts, M. (2017b). *MOHC HadGEM3-GC31-MM model output prepared for CMIP6 HighResMIP Version 20190901.* Retrieved from `http://doi.org/10.22033/ESGF/CMIP6.1902` doi: http://doi.org/10.22033/ESGF/CMIP6.1902

Roberts, M. (2018). *MOHC HadGEM3-GC31-HH model output prepared for CMIP6 HighResMIP Version 20190901.* Retrieved from `http://doi.org/10.22033/ESGF/CMIP6.445` doi: http://doi.org/10.22033/ESGF/CMIP6.445

Roberts, M. J., Baker, A., Blockley, E. W., Calvert, D., Coward, A., Hewitt, H. T., ... Vidale, P. L. (2019). Description of the resolution hierarchy of the global coupled HadGEM3-GC3.1 model as used in CMIP6 HighResMIP experiments. *Geoscientific Model Development Discussions*, *12*, 4999–5028. doi: 10.5194/gmd-2019-148

Roberts, M. J., Hewitt, H. T., Hyder, P., Ferreira, D., Josey, S. A., Mizielinski, M., & Shelly, A. (2016). Impact of ocean resolution on coupled air-sea fluxes and large-scale climate. *Geophysical Research Letters*, *43*(19), 10,430–10,438. doi: 10.1002/2016GL070559

Seo, H., Miller, A. J., & Norris, J. (2016). Eddy – Wind Interaction in the California Current System: Dynamics and Impacts. *Journal of Physical Oceanography*, *46*(1989), 439–459. doi: 10.1175/JPO-D-15-0086.1

Shan, X., Jing, Z., Gan, B., Wu, L., Chang, P., Ma, X., & Wang, S. (2020). Surface Heat Flux Induced by Mesoscale Eddies Cools the Kuroshio - Oyashio Extension Region. *Geophysical Research Letters*, 1–9. doi: 10.1029/2019GL086050

Small, R. J., Bryan, F. O., Bishop, S. P., Larson, S., & Tomas, R. A. (2020). What drives upper-ocean temperature variability in coupled climate models and observations? *Journal of Climate*, *33*(2), 577–596. doi: 10.1175/JCLI-D-19-0295.1

Small, R. J., Bryan, F. O., Bishop, S. P., & Tomas, R. A. (2019). Air-sea turbulent heat fluxes in climate models and observational analyses: What drives their variability? *Journal of Climate*, *32*(8), 2397–2421. doi:

10.1175/JCLI-D-18-0576.1

Small, R. J., DeSzoeke, S. P., Xie, S. P., O'Neill, L., Seo, H., Song, Q., ... Minobe, S. (2008). Air-sea interaction over ocean fronts and eddies. *Dynamics of Atmospheres and Oceans*, *45*(3-4), 274–319. doi: 10.1016/j.dynatmoce.2008.01.001

Storkey, D., Blaker, A. T., Mathiot, P., Megann, A., Aksenov, Y., Blockley, E. W., ... Sinha, B. (2018). UK Global Ocean GO6 and GO7: a traceable hierarchy of model resolutions. *Geoscientific Model Development*, *11*(8), 3187–3213. Retrieved from `https://www.geosci-model-dev-discuss.net/gmd-2017-263/` doi: 10.5194/gmd-2017-263

Valcke, S. (2013). The OASIS3 coupler: a European climate modelling community software. *Geoscientific Model Development*, *6*(2), 373–388. Retrieved from `http://www.geosci-model-dev.net/6/373/2013/` doi: 10.5194/gmd-6-373-2013

Valcke, S., Craig, T., & L., C. (2015). OASIS3-MCT User Guide. *OASIS3-MCT 3.0, Technical Report, TR/CMGC/15/38, CER- FACS/CNRS SUC URA No. 1875,*(May).

Villas Bôas, A. B., Sato, O. T., Chaigneau, A., & Castelão, G. P. (2015). The signature of mesoscale eddies on the air-sea turbulent heat fluxes in the South Atlantic Ocean. *Geophysical Research Letters*, *42*(6), 1856–1862. doi: 10.1002/2015GL063105

Wallace, J. M., Mitchell, T. P., & Deser, C. (1989). *The Influence of Sea-Surface Temperature on Surface Wind in the Eastern Equatorial Pacific: Seasonal and Interannual Variability* (Vol. 2) (No. 12). doi: 10.1175/1520-0442(1989)002⟨1492:tiosst⟩2.0.co;2

Walters, D., Boutle, I., Brooks, M., Melvin, T., Stratton, R., Vosper, S., ... Xavier, P. (2017). The Met Office Unified Model Global Atmosphere 6.0/6.1 and JULES Global Land 6.0/6.1 configurations. *Geoscientific Model Development*, *10*, 1487–1520. doi: 10.5194/gmd-10-1487-2017

Williams, K. D., Copsey, D., Blockley, E. W., Bodas-Salcedo, A., Calvert, D., Comer, R., ... Xavier, P. K. (2018). The Met Office Global Coupled Model 3.0 and 3.1 (GC3.0 and GC3.1) Configurations. *Journal of Advances in Modeling Earth Systems*, *10*(2), 357–380. doi: 10.1002/2017MS001115

Xie, S. P. (2004). *Satellite observations of cool ocean-atmosphere interaction* (Vol. 85) (No. 2). doi: 10.1175/bams-85-2-195

Yang, P., Jing, Z., & Wu, L. (2018). An Assessment of Representation of Oceanic Mesoscale Eddy-Atmosphere Interaction in the Current Generation of General Circulation Models and Reanalyses. *Geophysical Research Letters*, *45*(21), 11,856–11,865. doi: 10.1029/2018GL080678

Geophysical Research Letters

Supporting Information for

Air-Sea Turbulent Heat Flux Feedback over Mesoscale Eddies

Sophia Moreton [1], David Ferreira [1], Malcolm Roberts [2], Helene Hewitt [2]

1. University of Reading, UK

2. Met Office Hadley Centre, Exeter, UK

Contents of this file

Introduction

This supporting information provides more details of the filtering and composite averaging method, additional figures and a table of the number of eddy snapshots for each amplitude bin.

Text S1.

Filtering and composite averaging method

The high-pass filtered field is constructed by removing a low-passed field obtained from a Gaussian filtering of 20^0 zonally and 10^0 meridionally. The type of the filtering is important as it can change the strength of the anomaly within an eddy, and our approach differs from previous work e.g. Hausmann et al., (2012) and Frenger et al. (2013). We maintain a consistent strength of filtering across resolutions and variables, as well as for a regular and irregular NEMO grid, by applying grid point-dependent filtering.

Composite averaging includes for all eddies globally over one year, to effectively remove variability associated with changing oceanic and atmospheric conditions. The centre of the eddy is identified by the algorithm. A region around the eddy, 2.8 times the effective eddy radius (L_{eff}), is selected by identifying the nearest grid point to the eddy centre on either the ocean or atmospheric grid from the fields (THF, T_{air}, SST_O and SST_A). The 5.6 x 5.6 L_{eff} patch of a high-pass filtered variable (e.g. SST) is then extracted and normalized by L_{eff} in zonal and meridional directions. For ocean variables, interpolating the high-pass filtered patch to a high resolution grid converts from the irregular NEMO grid to a regular grid. The selected year of data for compositing for each model configuration is 4 or 5 years after the eddy tracking began in 1950 (or 1970 for N216-12):

N216_025 : 1955
N512_12 : 1954
N216_12 : 1975

For the results used in this study, rotating the snapshots before composite averaging made little difference. However when separating the eddies in each hemisphere a poleward shift can be observed in anticyclones, or an equatorward shift in cyclones, between the eddy centre and the maximum SST_O (or LHF) anomaly. By separating each hemisphere, this effectively produces a background northward SST gradient in the Northern Hemisphere, and a background southward SST gradient in the Southern Hemisphere. The phase shift, which can be observed in each model resolution, is consistent with observations and can be amplified in smaller amplitude eddies, where the monopole spatial structure changes to a dipole (Hausmann et al, 2012).

According to Hausmann et al., 2012 (their Appendix A), 2503 snapshots (averaged across all amplitudes and model resolutions) is enough to remove weather noise and obtain a robust average. It should be highlighted that, in the present study, the number of snapshots in the larger amplitude bins are far fewer, down to about 250 snapshots. The number of eddy snapshots used in each bin can be found in TableS1 below.

Assuming a normal distribution of data and using the student's t-test, 95% confidence intervals are supplied in Fig. 2 and 3 to find the confidence of the fitted linear regression line.

References

Hausmann U. and Czaja A., 2012, The observed signature of mesoscale eddies in sea surface temperature and the associated heat transport, Deep Sea Research Part 1: Oceanographic Research Papers, 70, 60-72, doi: 10.1016/j.dsr.2012.08.005

Frenger I., Gruber N., Knutti R. and Munnich M., 2013, Imprint of Southern Ocean eddies on winds, clouds and rainfall, Nature Geoscience Letters, 6, 608-612, doi: 10.1038/NGEO1863

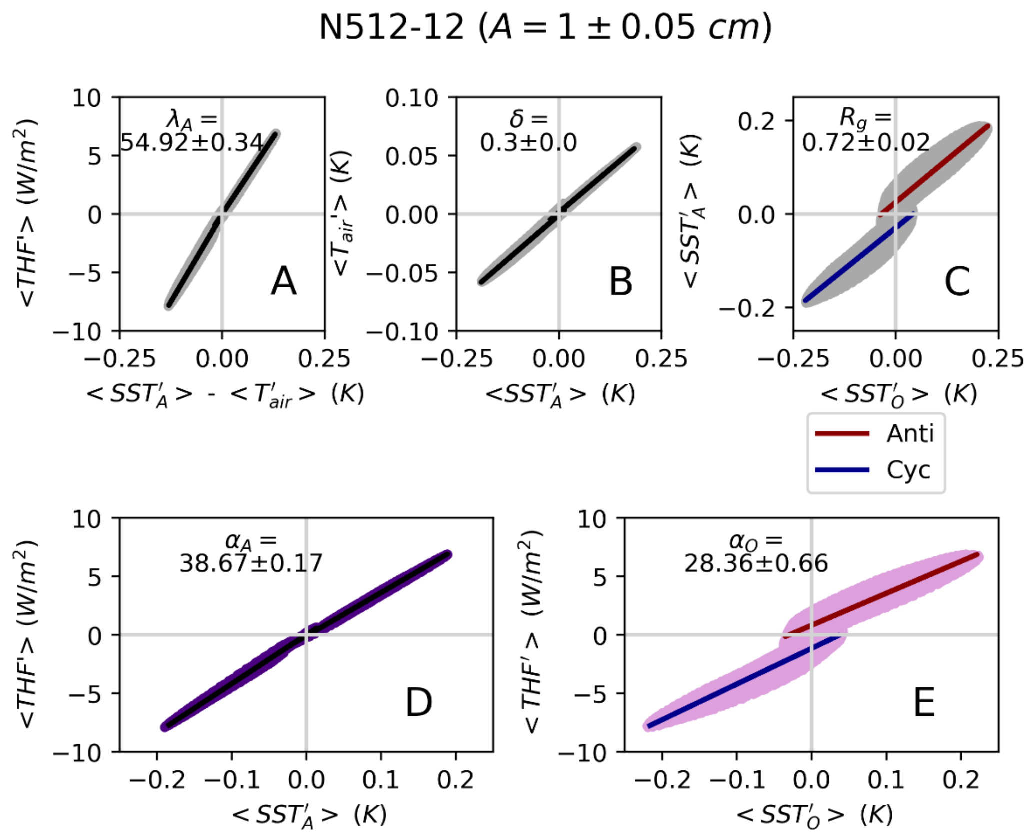

Figure S1. A repeat of Fig 2 for the smallest amplitude eddies from N512-12. Anticyclonic eddies are separated from cyclonic eddies due to different regression lines and plotted in red and blue, respectively.

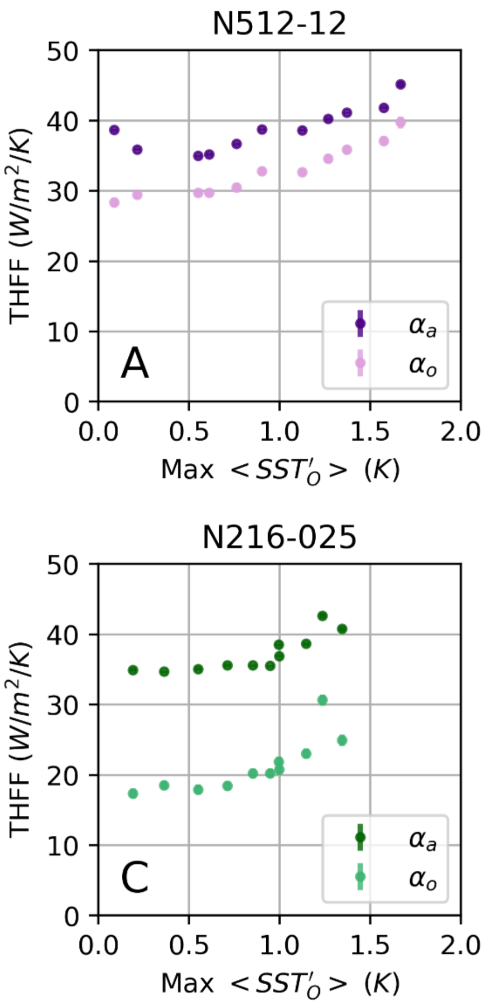

Figure S2. A repeat of Fig 3 plotting $\boldsymbol{\alpha_O}$ and $\boldsymbol{\alpha_A}$ as a function of the maximum SST_O anomaly, instead of eddy amplitude, for each configuration: N512-12, N216-12, and N216-025.

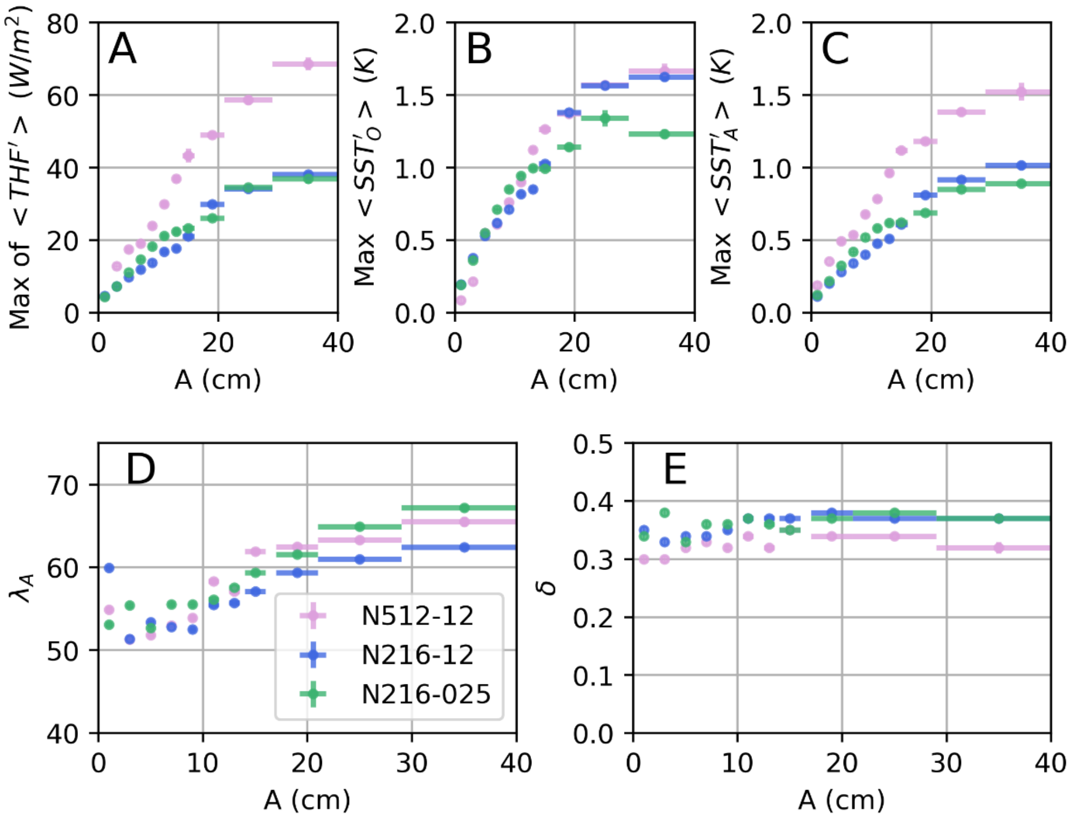

Figure S3. Scatter plots of (A) the maximum absolute THF (in W m^{-2}), (B) SST_O (in K) and (C) SST_A (in K) eddy composites, $\boldsymbol{\lambda_A}$ (D) and $\boldsymbol{\delta}$ (E) for each binned eddy amplitude (A, in cm). Results are shown for each configuration: N512-12, N216-12, and N216-025.

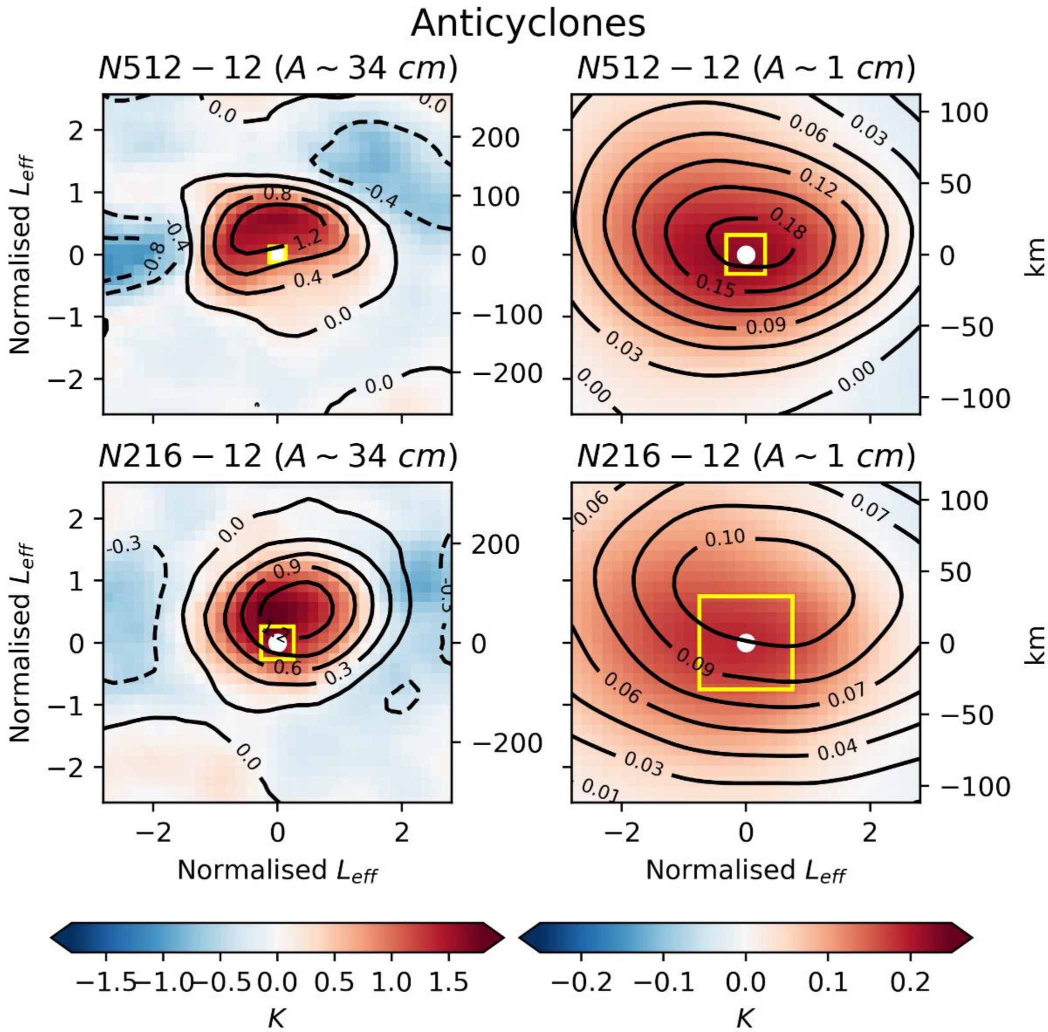

Figure S4. Composite maps of anti-cyclonic eddies with SST_O (colour) and SST_A (contours) anomalies (in K) for the large amplitude (A=34+/-6 cm) eddies (left) and the small amplitude (A=1+/-0.05 cm) eddies (right). Results for the N512-12 and N216-12 configurations are shown in the upper and lower rows, respectively. The yellow square represents the approximate horizontal grid resolution in the atmosphere at the mid-latitudes.

Amp	N216-025 (A)	N216-025 (C)	N216-12 (A)	N216-12 (C)	N512-12(A)	N512-12 (C)
1±0.05	5878	3228	8492	4487	10506	4992
3±0.05	5051	4300	6732	6084	5857	5734
5±0.05	1891	2232	2555	2998	1709	2367
7±0.1	1579	2142	2215	3119	1132	2021
9±0.2	1513	2142	2122	3158	1020	1793
11±0.5	1773	3440	2582	4702	1118	2254
13±0.5	1153	1926	1458	2799	715	1349
15±1	1254	2546	1909	3556	857	1704
19±2	1212	2151	1537	2858	847	1308
25±4	697	1934	1224	2427	502	1062
34±6	568	799	498	1355	248	257

Table S1. Number of eddy snapshots for each eddy amplitude bin (Amp) in cm, for each model resolution and polarity (anticyclonic, A or cyclonic, C).